Drug Design, Development and Therapy

Dovepress
Taylor & Francis Group

Open Access Full Text Article

ORIGINAL RESEARCH

Cyp3a4-Mediated in vitro Metabolism and in vivo Disposition of Lorlatinib in Rats

Cong Xie[1,2,*], Tongshu Guan[1,2,*], Jin Huang[1,2], Jiayu Chen[1,2], Yilei Li[1,2], Ping Zheng[1,2]

[1]Clinical Pharmacy Center, Nanfang Hospital, Southern Medical University, Guangzhou, People's Republic of China; [2]Department of Pharmacy, Nanfang Hospital, Southern Medical University, Guangzhou, People's Republic of China

*These authors contributed equally to this work

Correspondence: Yilei Li; Ping Zheng, Email lei@smu.edu.cn; zpm321@126.com

Drug Design, Development and Therapy downloaded from https://www.dovepress.com/
For personal use only.

Purpose: Lorlatinib, a third-generation inhibitor of anaplastic lymphoma kinase (ALK) and c-ros oncogene 1 (ROS1), undergoes extensive metabolism, with its disposition influenced by drug–drug interactions (DDIs). This study aimed to characterize its in vitro metabolism, in vivo pharmacokinetics (PK), tissue distribution, and the effects of cytochrome P450 3A4 (CYP3A4) modulation in rats.

Methods: Lorlatinib metabolism was investigated in human liver microsomes (HLM) and rat liver micro- somes (RLM) using ultra-high-performance liquid chromatography–tandem mass spectrometry (UHPLC–MS/MS) with selective CYP inhibitors. Pharmacokinetic (PK) studies were performed in Sprague–Dawley (SD) rats following oral and intravenous dosing, including coadministration with CYP3A4 inhibitors (voriconazole, itraconazole) and inducers (rifampicin, carbamazepine). Tissue distribution was assessed across major organs.

Results: In vitro assays confirmed CYP3A4 as the primary enzyme mediating lorlatinib metabolism, with distinct differences in kinetic parameters between HLM and RLM. In vivo, lorlatinib displayed nonlinear PK, low oral bioavailability (8.6%), and extensive first-pass metabolism. Voriconazole increased exposure [area under the curve from 0–24 h ($AUC_{(0-24h)}$)] by 120%, whereas rifampicin reduced it by 77%, demonstrating strong CYP3A4-dependent interactions. Lorlatinib distributed rapidly to highly perfused organs and achieved efficient brain penetration (brain-to-plasma ratio = 0.82).

Conclusion: Lorlatinib undergoes extensive CYP3A4-mediated metabolism, exhibits nonlinear PK, and shows poor oral bioavailability in rats. Significant interspecies differences between HLM and RLM emphasize the need for caution when translating preclinical findings. Coadministration with CYP3A4 modulators markedly altered systemic exposure, while effective brain penetration supports its therapeutic role in central nervous system (CNS) metastases.

Keywords: lorlatinib, CYP3A4 metabolism, enzyme kinetics, pharmacokinetics, tissue distribution

Introduction

Lorlatinib is a potent third-generation anaplastic lymphoma kinase (ALK) and c-ros oncogene 1 (ROS1) tyrosine kinase inhibitor (TKI) approved for the treatment of ALK-positive non-small cell lung cancer (NSCLC).[1,2] It is especially effective against central nervous system (CNS) metastases, addressing a key limitation of earlier ALK inhibitors.[1] Given to its significant clinical efficacy, lorlatinib is widely used in oncology practice.[3] However, cancer patients are frequently exposed to polypharmacy, and concomitant medications may precipitate drug–drug interactions (DDIs) that alter lorlatinib's therapeutic efficacy and safety profile.[4–6] Therefore, a detailed investigation of its DDIs is essential to better understand and manage its clinical pharmacology.

DDIs can substantially alter systemic exposure to anticancer agents, potentially resulting in subtherapeutic efficacy or increased toxicity.[7] Clinical and pharmacokinetic studies of several tyrosine kinase inhibitors have shown that coadministration with strong CYP3A inhibitors such as ketoconazole and itraconazole, or with potent inducers such as rifampicin, can markedly alter systemic exposure and, in some cases, increase the risk of adverse events or necessitate dose adjustment.[8,9] For instance, imatinib exposure increased by approximately 40% when combined with

Received: 4 September 2025
Accepted: 17 October 2025
Published: 25 October 2025

© 2025 Xie et al. This work is published and licensed by Dove Medical Press Limited. The full terms of this license are available at https://www.dovepress.com/terms.php and incorporate the Creative Commons Attribution – Non Commercial (unported, v4.0) License (http://creativecommons.org/licenses/by-nc/4.0/). By accessing the work you hereby accept the Terms. Non-commercial uses of the work are permitted without any further permission from Dove Medical Press Limited, provided the work is properly attributed. For permission for commercial use of this work, please see paragraphs 4.2 and 5 of our Terms (https://www.dovepress.com/terms.php).

ketoconazole,[10] brigatinib exposure nearly doubled with itraconazole,[11] and clinical reports have described itraconazole-related toxicity in patients receiving osimertinib.[12] As with other TKIs metabolized primarily by CYP3A, lorlatinib is prone to significant pharmacokinetic alterations when co-administered with CYP3A modulators.

For lorlatinib, co-administration with strong CYP3A4 inhibitors, such as itraconazole, has been shown to increase plasma AUC by approximately 42% and C_{max} by about 24%.[13] Conversely, potent CYP3A4 inducers, including rifampicin, dramatically reduce lorlatinib exposure to approximately 15% of control levels.[14] These pharmacokinetic alterations translate into clinically relevant consequences, as co-administration of lorlatinib with ritonavir has been associated with rapid elevations in liver function tests (LFTs) within 24–72 hours,[15,16] whereas co-administration with rifampicin has led to severe but self-limiting increases in transaminase levels in healthy volunteers.[14] Such findings emphasize that CYP3A-mediated DDIs not only modulate lorlatinib plasma concentrations but may also precipitate adverse reactions, highlighting the importance of investigating its metabolic characteristics both in vitro and in vivo.

Current evidence indicates that lorlatinib undergoes extensive biotransformation in vivo, primarily mediated by cytochrome P450 (CYP) 3A4 for oxidative Phase I metabolism and uridine 5′-diphospho-glucuronosyltransferase (UGT) 1A4 for N-glucuronidation in Phase II metabolism.[17,18] While minor contributions from CYP2C8, CYP2C19, CYP3A5, and UGT1A3 have not been detected, the relative contributions of these enzymes remain to be clarified.[3,19] This gap hampers a comprehensive understanding of its DDI liability.

To address this gap, in vitro liver microsomal systems are often employed.[20] Liver microsomes are extensively utilized in metabolic stability assays because they are easy to handle and contain a comprehensive array of drug-metabolizing enzymes. These enzymes encompass major CYP450 isoforms, flavin-containing monooxygenases, carboxylesterases, epoxide hydrolases, as well as UGTs.[21,22] This composition enables liver microsomes to closely mimic in vivo metabolic processes.[23,24] When combined with selective enzyme inhibitors, they can be used to identify the specific enzymes responsible for the major metabolic pathways of a compound, thereby aiding in the prediction of potential DDIs in humans.[7] Similar integrated strategies have been successfully applied to other anticancer agents, such as the TKIs canertinib[25] and amdizalisib, a PI3Kδ inhibitor,[26] facilitating dose optimization and informed management of potential DDIs. It is suggested to provide additional justification for studying the metabolism of lorlatinib, since it is the most recent ALK inhibitor approved by the FDA for NSCLC. Furthermore, the study by Zapata Dongo R. et al proposes that lorlatinib could overcome up to 53 amino acid mutations in ALK and might even be repurposed for other neoplasms.[27] This context increases the relevance of the present work, as it could provide solid foundations to explain the efficacy of lorlatinib in NSCLC. Therefore, a systematic investigation into lorlatinib's in vitro and in vivo metabolism is warranted, not merely to advance pharmacokinetic insights but also to establish the rationale for its safe and effective use in patients.

Accordingly, in the present study, we combined in vitro liver microsomal assays with in vivo pharmacokinetic experiments in rats to clarify the metabolic disposition of lorlatinib and to better predict its interaction potential in clinical settings. For the first time, we investigated interspecies variation in the in vitro metabolic stability of lorlatinib using human liver microsomes (HLM) and rat liver microsomes (RLM) to provide a comprehensive characterization of its disposition. We used an ultra-high-performance liquid chromatography–tandem mass spectrometry (UHPLC–MS/MS) method to determine the concentrations of lorlatinib and its metabolite M2a. Building on this foundational in vitro analysis, our investigation extended to in vivo studies. We determined its pharmacokinetic profile after a single oral dose in rats, evaluated its drug-drug interaction potential with potent CYP3A4 inhibitors (itraconazole, voriconazole) and inducers (rifampicin, carbamazepine), and quantified its tissue distribution with an emphasis on brain penetration and major organ biodistribution. Collectively, these objectives sought to establish a foundational understanding of lorlatinib's metabolic fate, systemic exposure, interaction risks, and tissue accessibility.

Materials and Methods

Drugs and Reagents

Lorlatinib (purity 98%, CAS No. 1454846–35-5) was supplied by Aladdin Industrial Corporation (Shanghai, China). Voriconazole (≥98%, CAS No. 137234–62-9), itraconazole (≥98%, CAS No. 84625–61-6), rifampicin (97%, CAS

No. 13292–46-1), and carbamazepine (>99%, CAS No. 298–46-4) were also purchased from Aladdin. Gefitinib (≥99%, CAS No. 184475–35-2), obtained from the same vendor, served as the internal standard (IS). Methanol and acetonitrile of analytical grade were obtained from Aladdin, while ultrapure water was produced in-house using a Pall purification system. All other reagents were of analytical grade.

Experimental Animals

Male Sprague–Dawley (SD) rats (200 ± 20 g, 6–8 weeks old) were provided by the Experimental Animal Center of Southern Medical University (Guangzhou, China; license No. SCXK 2021–0041). Animals were housed under controlled laboratory conditions (25 ± 2 °C, 50 ± 5% relative humidity, 12 h light/dark cycle) and acclimated for one week before the start of the study. Rats were fasted for 12 h prior to drug administration. All animal procedures were conducted in compliance with the National Institutes of Health Guide for the Care and Use of Laboratory Animals. Ethical approval was granted by the Ethics Committee of Southern Medical University (Approval No. SMUL202410030), and all protocols were reviewed and approved by the Institutional Animal Care and Use Committee of Southern Medical University.

Chromatography and Conditions

UHPLC–MS/MS analysis was carried out on an Agilent 1290 Infinity II LC system coupled with an Agilent 6495 triple quadrupole mass spectrometer. Separation was achieved using an Eclipse Plus C18 column (2.1 × 50 mm, 1.8 μm; Agilent) maintained at 30 °C. The mobile phase consisted of acetonitrile (solvent A) and 0.1% formic acid in water (solvent B), delivered at a flow rate of 0.3 mL/min. The gradient program was as follows: 0–0.5 min, 10% A; 0.5–3.0 min, 10–80% A; 3.0–4.0 min, 80% A; 4.0–4.1 min, 80–10% A; and 4.1–5.0 min, 10% A, with a total runtime of 5 min. Detection was performed on an Agilent Jet Stream electrospray ionization (AJS-ESI) source in positive ion mode. The monitored ion transitions were lorlatinib m/z 407 → 228 (fragmentor 166 V, collision energy 30 eV), IS m/z 447 → 128 (fragmentor 166 V, collision energy 20 eV), and M2a m/z 393 → 180 (fragmentor 166 V, collision energy 20 eV). Source conditions were set as follows: gas temperature, 200 °C; nebulizer pressure, 20 psi; gas flow, 14 L/min; capillary voltage, 3000 V; and corona current, 0.13 μA. Data collection and processing were conducted using MassHunter software (version B.10.1.67, Agilent). The UHPLC-MS/MS method validation details, including accuracy, precision, and linearity, are provided in the Supplementary Tables 1–4. The ultra-performance liquid chromatography–quadrupole time-of-flight mass spectrometry (UPLC-QTOF-MS) system from Waters was used to analyze the metabolite M2a, and representative spectra and chromatograms are included in the Supplementary Figures 1 and 2.

In vitro Experiments

Enzyme Kinetics

Human liver microsomes (HLM) and rat liver microsomes (RLM) were supplied by IPHASE BIOSCIENCES Co., Ltd. (Suzhou, China). Incubations were carried out in a final volume of 190 μL containing 100 mM PBS (pH 7.4), lorlatinib at various concentrations, and microsomal protein (0.05 mg/mL). For RLM, lorlatinib concentrations ranged from 0.001 to 4 mM (0.001, 0.01, 0.05, 0.25, 1, 1.5, 2, 2.5, 3, and 4 mM), while for HLM, the range was 0.001–4 mM (0.001, 0.01, 0.05, 0.10, 0.25, 1, 1.5, 2, 2.5, and 4 mM). After a 5-min equilibration at 37 °C, reactions were initiated by the addition of 12 μL of NADPH regenerating system (10 μL Solution A + 2 μL Solution B). Mixtures were incubated for 60 min and then terminated by adding 600 μL of acetonitrile containing the internal standard (IS, 50 ng/mL). Samples were vortexed briefly, centrifuged at 13,000 rpm for 30 min at 4 °C, and 100 μL of the supernatant was analyzed by UHPLC–MS/MS for lorlatinib metabolite quantification and determination of Michaelis–Menten kinetics (K_m). All assays were conducted using the IPHASE I Metabolic Stability Research Kit (IPHASE BIOSCIENCES, Suzhou, China) following the manufacturer's protocol.

Enzyme Phenotyping

CYP450 phenotyping of lorlatinib was conducted in pooled human (HLM) and rat liver microsomes (RLM) using the IPHASE CYP450 Metabolic Phenotype Research Kit (Chemical Inhibition Method, V1.5; IPHASE Biosciences, Suzhou,

China). Each incubation (200 μL total volume) contained 100 mM PBS (pH 7.4), microsomal protein (0.5 mg/mL), an NADPH-regenerating system (kit solutions A and B), lorlatinib as substrate, and a selective CYP isoform inhibitor. Substrate concentrations were 10 μM for HLM and 1 μM for RLM, approximating their respective K_m values. Lorlatinib was prepared from a 10 mM DMSO stock, with the final solvent content maintained below 1% (v/v).

The following inhibitors were used at isoform-selective concentrations: α-naphthoflavone (200 μM, CYP1A2), sertraline (25 μM, CYP2B6), montelukast (500 μM, CYP2C8), sulfaphenazole (1 μM, CYP2C9), nootkatone (25 μM, CYP2C19), quinidine (10 μM, CYP2D6), and ketoconazole (1 μM, CYP3A4). Reaction mixtures were pre-equilibrated at 37 °C for 5 min (without microsomes), after which HLM or RLM were added to initiate the reaction. Incubations were carried out at 37 °C for isoform-specific times (CYP1A2, 30 min; CYP2B6, 30 min; CYP2C8, 5 min; CYP2C9, 20 min; CYP2C19, 30 min; CYP2D6, 10 min; CYP3A4, 10 min). Reactions were terminated with three volumes of ice-cold acetonitrile containing internal standard, and protein was removed by centrifugation. The relative contributions of individual CYP isoforms were assessed using the substrate depletion approach, whereby the rate of lorlatinib disappearance in the presence of selective CYP inhibitors was measured to estimate enzymatic activity, following the kit protocol.

In vivo Pharmacokinetic Experiments

Serum Sample Preparation

A 100 μL aliquot of plasma was combined with 300 μL of an acetonitrile solution containing 50 ng/mL internal standard (IS) and vortex-mixed for 3 minutes. Lorlatinib was extracted by centrifuging the mixture at 13,000 rpm for 20 minutes at 4 °C. Subsequently, 320 μL of the upper organic layer was transferred to a 1.5-mL microcentrifuge tube and evaporated to dryness under a gentle stream of nitrogen at –70 °C. The dried residue was reconstituted in 100 μL of a 50:50 (v/v) acetonitrile/water solution followed by vortex mixing for 3 minutes. After a second centrifugation step (13,000 rpm, 20 minutes, 4 °C), 70 μL of the supernatant was collected into a vial, and 1 μL was injected into the UHPLC–MS/MS system for analysis.

Tissue Sample Pretreatment

For tissue samples, approximately 50 mg of tissue was weighed and homogenized in 0.45 mL of ice-cold physiological saline (0.9%). The homogenate was centrifuged at 13,000 rpm for 20 minutes at 4 °C to obtain the supernatant. A 100 μL aliquot of the supernatant was then treated with 500 μL of acetonitrile containing 50 ng/mL IS, vortex-mixed, and centrifuged. From the resulting mixture, 520 μL of the organic phase was transferred to a 1.5-mL microcentrifuge tube and evaporated to dryness at –70 °C. In the pharmacokinetic study, this homogenization and extraction procedure was consistently repeated across all tissue samples.

PK Study

Forty-eight male Sprague-Dawley (SD) rats were randomly divided into nine groups (n = 6 per group) and received the following treatments: control group, single dose of lorlatinib (10 mg/kg); voriconazole group, single dose of voriconazole (20 mg/kg) administered 30 min before the experiment; itraconazole group, single dose of itraconazole (20 mg/kg) administered 30 min before the experiment; rifampicin group, daily dose of rifampicin (50 mg/kg) administered over 7 days; carbamazepine group, daily dose of carbamazepine (50 mg/kg) administered over 7 days; low-dose group, single dose of lorlatinib (5 mg/kg); and high-dose group, single dose of lorlatinib (50 mg/kg). All drug solutions were made up in 0.5% carboxymethylcellulose sodium. The voriconazole and itraconazole groups received 10 mg/kg lorlatinib orally 30 min after oral administration of voriconazole and itraconazole. Following 7 consecutive days of daily oral gavage with 50 mg/kg rifampicin or carbamazepine, animals in the rifampicin and carbamazepine groups were administered a single dose of lorlatinib (10 mg/kg) orally on the 8th day. The dosing regimens for CYP inhibitors were selected according to established rodent pharmacokinetic studies,[28–30] and the 7-day pretreatment for rifampicin and carbamazepine was adopted to achieve stable enzyme induction as supported by previous reports.[31,32]

To determine absolute bioavailability, six SD rats were weighed and received a single dose of lorlatinib (1 mg/kg) via caudal intravenous injection. Thereafter, a 100-μL blood sample was harvested in 1.5-mL heparinized tubes through the

retroorbital plexus at 0.083, 0.167, 0.25, 0.333, 0.5, 1, 2, 4, 6, 8, 12, and 24 h. Plasma was collected by centrifuging at 6,000 rpm at 4 °C for 10 min before transferring to another 1.5-mL Eppendorf microcentrifuge tube. Samples were stored at −80 °C before further analysis.

Tissue Distribution Study

Forty-eight male Sprague-Dawley rats were randomly assigned to eight experimental groups (n = 6 per group) and their body weights were recorded. Each animal was administered a single oral dose of lorlatinib (10 mg/kg). At predetermined time points (0.0833, 0.25, 0.5, 1, 2, 4, 6, and 24 h) after administration, the rats were euthanized by cervical dislocation. The heart, liver, spleen, lungs, kidneys, stomach, cecum, colon, and brain were promptly excised. Each tissue was perfused with ice-cold physiological saline (0.9%) to remove residual blood, gently blotted dry on filter paper, and subsequently stored at −80 °C pending further analysis.

Molecular Docking Analysis

The three-dimensional structure of CYP3A4 (PDB ID: 00009bv5) was obtained from the Protein Data Bank (https://www.rcsb.org/). The structures of lorlatinib (PubChem CID: 71731823), voriconazole (PubChem CID: 71616), and itraconazole (PubChem CID: 55283) were retrieved from PubChem (https://pubchem.ncbi.nlm.nih.gov/). Protein preprocessing was performed in PyMOL by removing chains B and C, the co-crystallized ligand, and all water molecules. Hydrogen atoms were subsequently added using AutoDock Tools 1.5.6. Semi-flexible molecular docking was carried out with AutoDock Vina, generating up to 20 docking conformations for each ligand. Docking poses were clustered with a root mean square deviation (RMSD) threshold of 0–2 Å, and the representative pose with the lowest binding energy from the most populated cluster was selected. The final binding conformations were visualized and analyzed using PyMOL.

Statistical Analysis

The mean plasma concentration–time profile was generated using Prism 10.0 (GraphPad Software Inc., San Diego, USA). Pharmacokinetic (PK) parameters for lorlatinib were derived by non-compartmental analysis (NCA) implemented in Drug and Statistics Software (DAS, version 2.0). All statistical comparisons were conducted with SPSS 19.0 using one-way ANOVA followed by Dunnett's post hoc test. A p-value less than 0.05 was considered statistically significant.

The extent of lorlatinib penetration into target tissues was assessed by calculating the total tissue-to-plasma partition coefficient (Kp), defined as the ratio of the area under the concentration–time curve (AUC) in tissue to that in plasma, using the following equation:

$$Kp = \mathrm{AUC_}(0-\infty), \cdot\mathrm{tissue}/\mathrm{AUC_}(0-\infty), \cdot\mathrm{plasma}$$

The absolute bioavailability (F) of lorlatinib in rats was derived using the formula:

$$F(\%) = \frac{\mathrm{AUC_{oral}}/\mathrm{Dose_{oral}}}{\mathrm{AUC_{IV}}/\mathrm{Dose_{IV}}} \times 100$$

where AUC $_{oral}$ and AUC $_{iv}$ represent the area under the concentration-time curve from 0 to infinity after oral and intravenous administration of lorlatinib, respectively. Similarly, Dose $_{oral}$ and Dose $_{iv}$ represent the oral and intravenous administration doses, respectively.

Results

In vitro Metabolism

Metabolite Identification

An UHPLC-MS/MS method for the quantification of lorlatinib in plasma and tissue homogenates was developed and validated. The method specificity was enhanced through optimization of mass spectrometric conditions in Supplementary Tables 1–4. Acetonitrile was selected as the protein precipitation solvent, which resulted in minimal endogenous

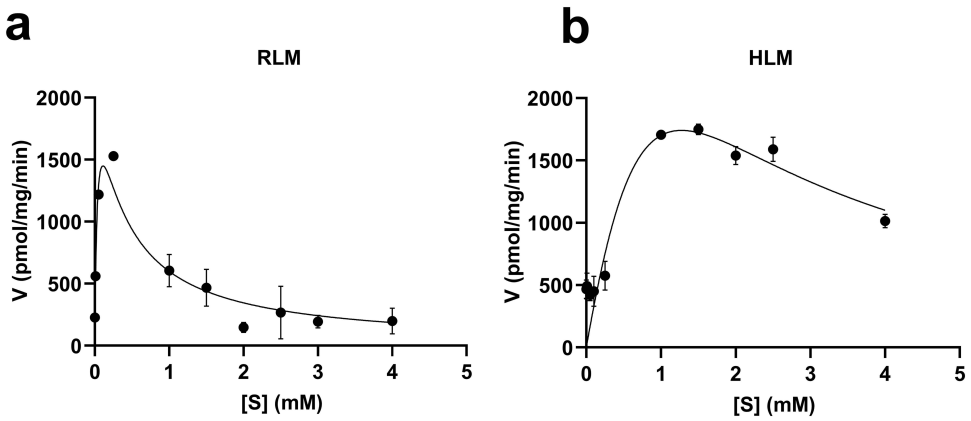

Figure 1 Kinetics analysis of lorlatinib demethylated (M2a) in rat liver microsomes (RLM) (**a**) and human liver microsomes (HLM) (**b**). The microsomal enzyme incubation assay was performed as indicated in the methods section. For RLM and HLM, K_m and V_{max} for lorlatinib demethylated (M2a) were calculated using GraphPad Prism 10.0 software using the following equation to describe substrate inhibition. Date points represent mean ± SD of three experiments performed in triplicate.

interference and efficient extraction of the analyte. The total analytical run time was approximately 4 min, with retention times of approximately 2.283, 2.122, and 2.051 min for lorlatinib, metabolite M2a, and the IS, respectively.

Kinetic Analysis of Lorlatinib

The incubation of lorlatinib with RLM and HLM for preliminary kinetic analysis produced an atypical metabolite formation curve for M2a. The observed trend was inconsistent with classical Michaelis-Menten kinetics but aligned with a model of substrate inhibition, where a drug, at elevated concentrations, impedes its own metabolism by binding to a non-catalytic inhibitory site on the enzyme[33] (Figure 1a and b).

The enzyme kinetic parameters, K_m, V_{max}, C_{lint}, and K_i values, are shown in Table 1. The metabolism of lorlatinib in RLM showed a low K_m value (0.035±0.013 mM) and a Vmax of 2389.40±1595.00 pmol/mg/min. Although the maximal velocity was moderate, the markedly reduced K_m resulted in a high intrinsic clearance (CL_{int} = 68.27 μL/min/mg protein), reflecting strong catalytic efficiency. Substrate inhibition was observed with a K_i of 0.339 mM, suggesting that excessive substrate concentrations could suppress the metabolic rate in rats.In the meantime,the metabolism of lorlatinib in HLM showed a higher V_{max} (8704 ± 2839.00 pmol/mg/min) but was accompanied by a much higher K_m (2.552 ± 0.509 mM), leading to a considerably lower CL_{int} (3.41 μL/min/mg protein) (Table 1). Substrate inhibition was also detected, with a K_i of 0.638 mM. Compared with RLM, the higher K_m in HLM indicates reduced substrate affinity, which may translate into slower metabolic turnover and greater in vivo accumulation of the parent drug. Such interspecies differences suggest that human metabolic capacity for lorlatinib is relatively limited, which may influence systemic exposure and tolerability in patients. These findings underscore the importance of considering species-specific metabolic profiles when extrapolating preclinical data to clinical settings.

Enzyme Phenotyping

To further investigate the interspecies differences in CYP-mediated metabolism between RLM and HLM, we assessed the inhibitory effects of selective chemical inhibitors. As shown in Figure 2, the major metabolic pathways indeed

Table 1 Kinetic Parameters of Lorlatinib Metabolism in Rat Liver Microsomes (RLM) and Human Liver Microsomes (HLM)

Species	K_m (mM)	V_{max} (pmol/mg/min)	C_{lint} (μL/min/mg)	K_i (mM)	Kinetic Mechanism Model
RLM	0.035±0.013	2389.40±1595.00	68.27	0.339	SI
HLM	2.552±0.509	8703.57±2839.00	3.41	0.638	SI

Notes: Values are expressed as mean ± SD (n = 3).
Abbreviations: RLM, rat liver microsomes; HLM, human liver microsomes; K_m, Michaelis–Menten constant; V_{max}, maximum velocity; C_{lint}, intrinsic clearance; K_i, inhibition constant; SI, substrate inhibition model.

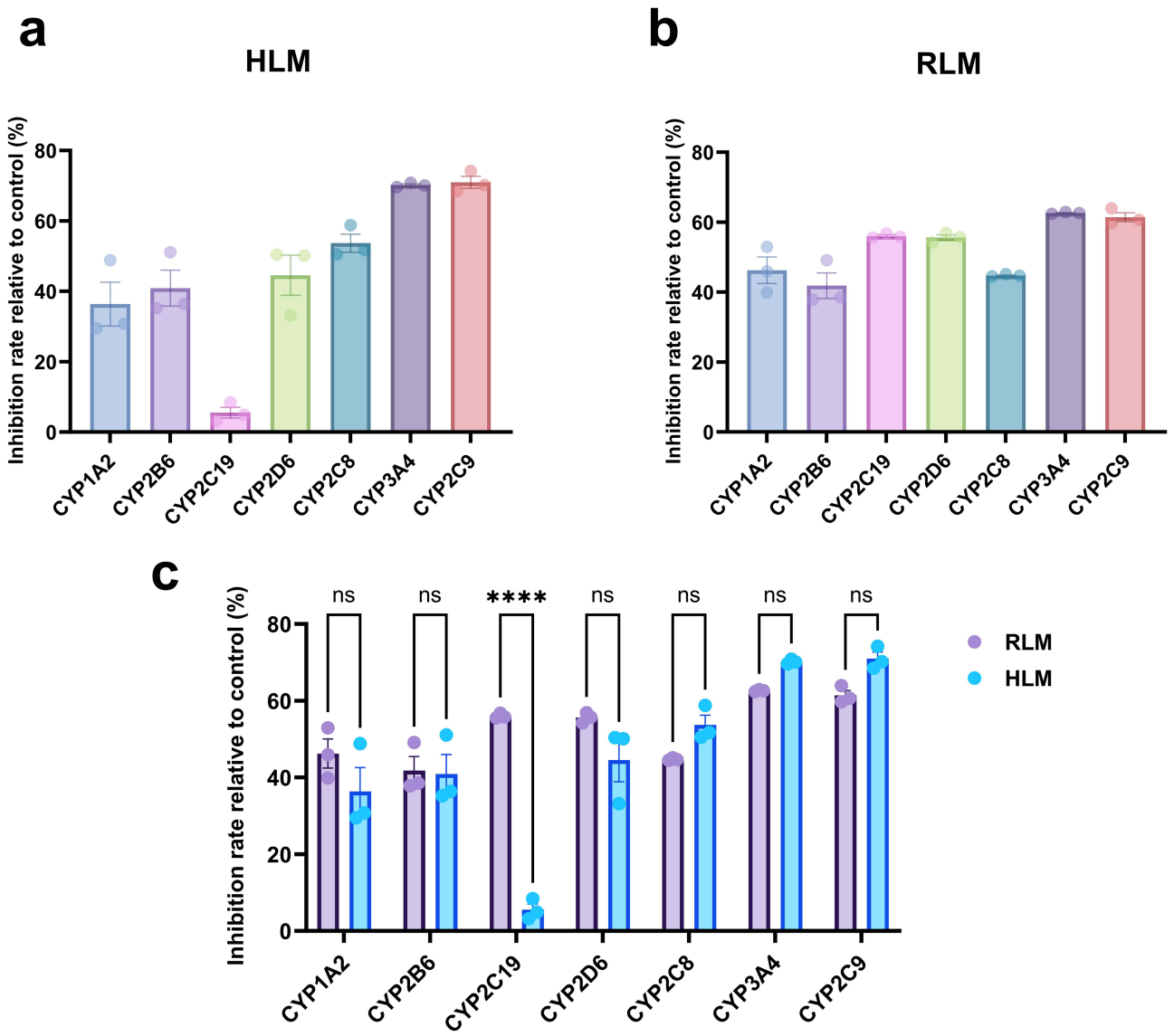

Figure 2 Comparative inhibition of lorlatinib metabolism in rat and human liver microsomes. (**a**) Relative inhibition rates of lorlatinib metabolism in rat liver microsomes (RLM) by selective CYP inhibitors. (**b**) Relative inhibition rates of lorlatinib metabolism in human liver microsomes (HLM) by selective CYP inhibitors. (**c**) Comparison of overall inhibition patterns between RLM and HLM analyzed by one-way ANOVA. Data are presented as mean ± SD (n = 3). $p < 0.05$ indicates significant difference between groups.

differed between RLM and HLM. CYP3A exhibited the highest inhibition rates in both systems (62.5% in RLM and 70.8% in HLM), indicating that it is the primary enzyme involved in lorlatinib metabolism. In contrast, the contributions of other CYP isoforms varied substantially between the two species. In our study, CYP2C19 displayed a moderate contribution in RLM, whereas its role was negligible in HLM. These findings suggest that the observed differences are mainly attributable to interspecies variation in CYP expression profiles and kinetic parameters.

In vivo Metabolism

Effects of CYP3A4 Inhibitors on the PK of Lorlatinib

The mean plasma concentration-time profiles of lorlatinib following co-administration with CYP3A4 inhibitors are presented in Figure 3, and the corresponding pharmacokinetic parameters were summarized and compared in the Table 2 and Supplementary Figure 3. Pretreatment with either voriconazole or itraconazole resulted in a significant increase in the systemic exposure of lorlatinib. The mean ± standard deviation (SD) of the mean C_{max} concentrations were 565.74 ±

https://doi.org/10.2147/DDDT.S565228

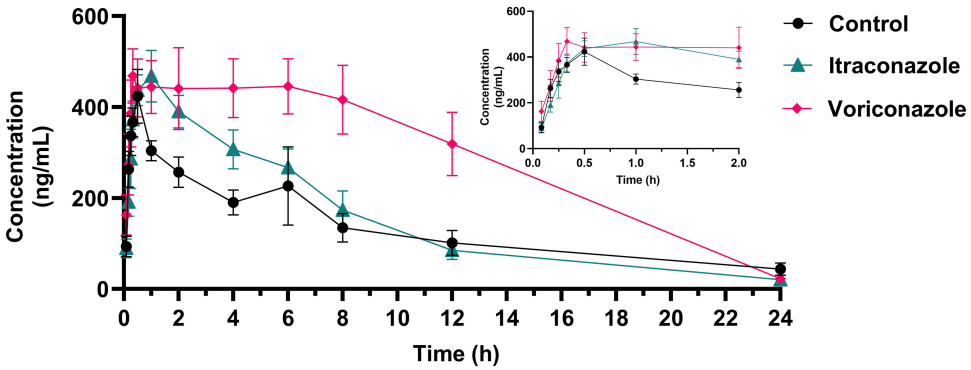

Figure 3 The mean plasma concentration time profile of lorlatinib after oral administration of voriconazole and itraconazole (20 mg/kg, n = 6). The detailed plasma concentration-time profiles of lorlatinib during the initial 2 h period following administration was also showed. Error bars represent ± SD for concentrations.

171.36 ng/mL and 508.16 ± 124.05 ng/mL in the voriconazole and itraconazole groups, respectively, compared with 468.02 ± 165.79 ng/mL in the control group, representing increases of 20.88% and 8.58%, respectively. Notably, voriconazole led to a significant increase of 120.39% in the $AUC_{(0–24h)}$, with values rising from 3,162.09 ± 1,491.41 ng/mL in the control group to 6,969.08 ± 2,844.69 ng/mL (P = 0.009; 95% CI 1012.472 to 6601.514). Itraconazole caused a 15% increase in the $AUC_{(0–24h)}$ to 3,636.34 ± 1,223.35 ng h/mL (P = 0.693; 95% CI −2066.2 to 3014.7). These results indicate that voriconazole has a more potent inhibitory effect on lorlatinib metabolism than itraconazole. Furthermore, lorlatinib clearance in the voriconazole and itraconazole groups was 0.002 ± 0.001 L/h and 0.003 ± 0.001 L/h, respectively, with a notable reduction of approximately 50% and 25% from that in the control groups (0.004 ± 0.003 L/h). The apparent volume of distribution ($V_{z/F}$) values for lorlatinib in the voriconazole and itraconazole groups was respectively 70.27% and 48.65% lower than that in the control group.

In addition, the value of mean residence time from time zero to infinity ($MRT_{(0–\infty)}$) decreased from 11.72 ± 5.56 h in the control group to 8.11 ± 0.53 h (P = 0.14, 95% CI −1.3 to 8.5) and 6.79 ± 1.37 h (P = 0.045, 95% CI 0.1 to 9.8) in the voriconazole and itraconazole groups, respectively. These results suggest that voriconazole and itraconazole inhibit the metabolism of lorlatinib, enhancing its bioavailability and systemic exposure by suppressing CYP3A4 activity.

Effects of CYP3A4 Inducers on the PK of Lorlatinib

Following the administration of lorlatinib with or without the CYP3A4 inducers rifampicin and carbamazepine, the mean plasma concentration-time profiles were assessed (Figure 4), and the pharmacokinetic parameters were compared and

Table 2 The Main Pharmacokinetic Parameters of Lorlatinib After Co-Administration with Voriconazole and Itraconazole (20 mg/kg, n = 6)

Parameters	Control	Voriconazole	Itraconazole
$t_{1/2}$ (h)	8.82±3.97	5.53±4.02	4.68±1.27
T_{max} (h)	1.36±2.28	2.15±2.98	0.85±0.54
$CL_{z/F}$ (L/h)	0.004±0.003	0.002±0.001	0.003±0.001
$V_{z/F}$ (L/kg)	0.037±0.011	0.011±0.007*	0.019±0.006*
C_{max} (ng/mL)	468.02±165.79	565.74±171.36	508.16±124.05
$AUC_{(0–24h)}$ (ng h/mL)	3162.09±1491.41	6969.08±2844.69*	3636.34±1223.35
$AUC_{(0-\infty)}$ (ng h/mL)	3837.13±2157.00	7499.02±2788.19*	3772.06±1331.97
$MRT_{(0–24h)}$ (h)	7.16±1.85	7.72±0.54	5.90±1.01
$MRT_{(0-\infty)}$ (h)	11.72±5.56	8.11±0.53	6.79±1.37*

Notes: *P < 0.05, compared with control group with lorlatinib alone; Values are expressed as mean ± SD. $t_{1/2}$, half-life; Tmax, time to reach maximum plasma concentration; CLz/F, apparent oral clearance; Vz/F, apparent volume of distribution after oral administration; Cmax, maximum plasma concentration; $AUC_{(0–24h)}$, area under the plasma concentration–time curve from 0 to 24 h; $AUC_{(0-\infty)}$, area under the plasma concentration–time curve from time zero to infinity; $MRT_{(0–24h)}$, mean residence time from 0 to 24 h; $MRT_{(0-\infty)}$, mean residence time from time zero to infinity.

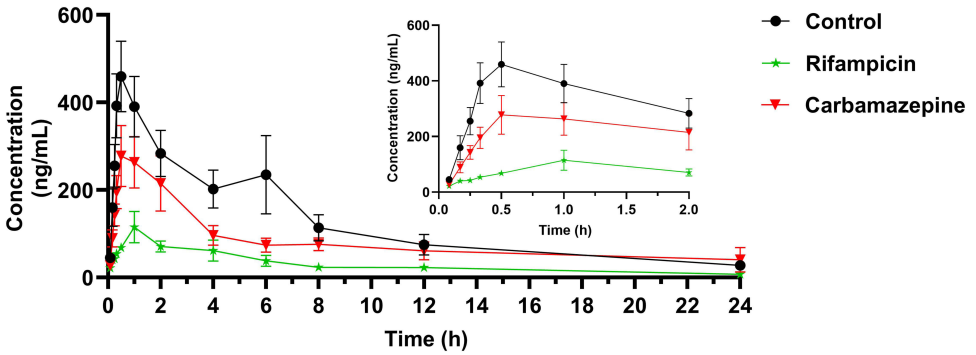

Figure 4 The mean plasma concentration time profile of lorlatinib after oral administration of multiple doses of rifampicin and carbamazepine for consecutive 7 days (50 mg/kg, n = 6). The detailed plasma concentration-time profiles of lorlatinib during the initial 2 h period following administration was also showed. Error bars represent ±SD for concentrations.

analyzed (Table 3 and Supplementary Figure 4). Administration of 50 mg/kg rifampicin daily over 7 days prior to a single 10 mg/kg dose of lorlatinib led to significant reductions in lorlatinib exposure levels. The C_{max}, $AUC_{(0–24h)}$, and $AUC_{(0-\infty)}$ were 140.08 ± 79.42 ng/mL, 723.59 ± 235.72 ng h/mL, and 755.59 ± 243.07 ng h/mL, respectively. These values indicate substantial decreases of 70.07%, 77.12%, and 80.31%, respectively, compared with administration of lorlatinib without CYP3A4 inducers. Furthermore, there was a marked increase in the lorlatinib clearance (0.004 ± 0.003 L/h to 0.015 ± 0.006 L/h; Table 3) when administered in the presence of rifampicin. Therefore, co-administration of rifampicin significantly altered the PK profile of lorlatinib, highlighting the substantial inductive effect of rifampicin on CYP3A4 activity.

Daily administration of 50 mg/kg carbamazepine over 7 consecutive days prior to administration of a single 10 mg/kg dose of lorlatinib resulted in a modest reduction in the plasma exposure of lorlatinib. C_{max} was 375.82 ±146.20 ng/mL in the carbamazepine group compared with 468.02 ± 165.79 ng/mL in the control group, a reduction of approximately 19.70%. The $AUC_{(0–24h)}$ in the carbamazepine group was 1,953.51 ± 853.11 ng h/mL, which represents a 38.22% reduction from that in the control group (3,162.09 ± 1,491.41 ng h/mL). The $AUC_{(0-\infty)}$ also showed a decrease of 30.41%, with values of 2,670.38 ± 2,052.47 ng h/mL in the carbamazepine group versus 3,837.13 ± 2,157.00 ng h/mL in the control group. Carbamazepine co-administration also increased lorlatinib clearance from 0.004 ± 0.003 L/h to 0.006 ± 0.003 L/h. However, this difference was not statistically significant (P = 0.694, 95% CI 0.0043 to 0.0080), suggesting that carbamazepine has a less pronounced induction effect on CYP3A4 activity than rifampicin.

Table 3 The Main Pharmacokinetic Parameters of Lorlatinib After Co-Administration with Rifampicin and Carbamazepine (n = 6)

Parameters	Control	Rifampicin	Carbamazepine
$t_{1/2}$ (h)	8.82±3.97	4.64±1.24	7.84±3.59
T_{max} (h)	1.36±2.28	1.24±1.41	0.72±0.31
$CL_{z/F}$ (L/h)	0.004±0.003	0.015±0.006*	0.006±0.003
$V_{z/F}$ (L/kg)	0.037±0.011	0.095±0.032*	0.053±0.024
C_{max} (ng/mL)	468.02±165.79	140.08±79.42*	375.82±146.20
$AUC_{(0–24h)}$ (ng h/mL)	3162.09±1491.41	723.59±235.72*	1953.51±853.11
$AUC_{(0-\infty)}$ (ng h/mL)	3837.13±2157.00	755.59±243.07*	2670.38±2052.47
$MRT_{(0–24h)}$ (h)	7.16±1.85	7.02±1.38	7.45±2.54
$MRT_{(0-\infty)}$ (h)	11.72±5.56	8.83±1.89	12.11±9.53

Notes: *P < 0.05, compared with control group with lorlatinib alone; Values are expressed as mean ± SD.

https://doi.org/10.2147/DDDT.S565228

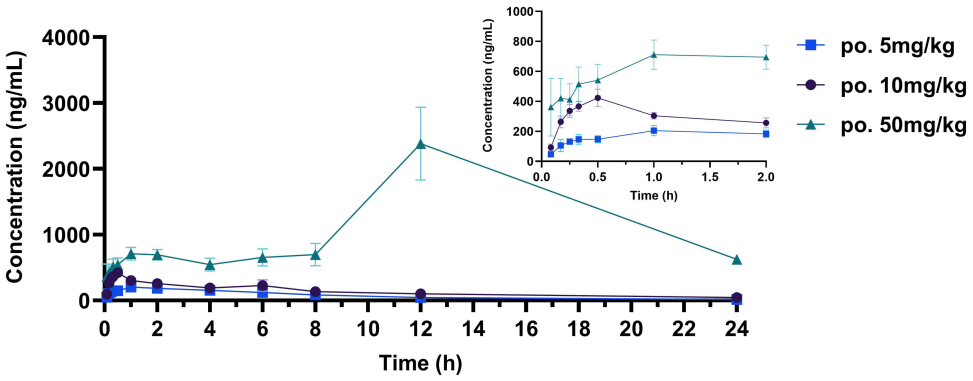

Figure 5 The mean plasma concentration time profile of lorlatinib after oral administration of low, medium and high dose (5 mg/kg, 10 mg/kg and 50 mg/kg) in rats. The detailed plasma concentration-time profiles of lorlatinib during the initial 2 h period following administration was also showed. Error bars represent ± SD for concentrations.

Effect of Dose Escalation on the PK of Lorlatinib

The plasma concentration–time profiles of lorlatinib following oral administration at 5, 10, and 50 mg/kg in rats are shown in Figure 5, with pharmacokinetic parameters summarized in Table 4. Dose escalation from 5 to 50 mg/kg produced a dose-dependent trend in systemic exposure.

The $AUC_{(0–24h)}$ values at the low, medium, and high doses were 1,780.60 ± 573.68, 3,162.09 ± 1,491.41, and 24,756.38 ± 5,906.92 ng h/mL, respectively, and the corresponding C_{max} values were 218.29 ± 72.67, 468.02 ± 165.79, and 2,484.98 ± 1,363.21 ng/mL. While lorlatinib exposure increased approximately dose-proportionally at the lower doses, the 50 mg/kg dose exhibited a pronounced deviation from proportionality. Mean clearance values decreased from 0.003 ± 0.001 and 0.004 ± 0.003 L/h at the lower doses to 0.001 ± 0.001 L/h at the highest dose, consistent with reduced clearance at higher systemic exposure. These results indicate that lorlatinib pharmacokinetics in rats demonstrate a dose-dependent trend toward nonlinearity at 50 mg/kg, potentially reflecting partial saturation of metabolic enzymes or transporter-mediated processes. However, due to species differences, these findings cannot be directly extrapolated to humans, and identifying the dose at which nonlinear metabolism occurs in patients requires further studies with broader dose ranges and more rigorous experimental design.

Absolute Oral Bioavailability

The mean plasma concentration–time curve of lorlatinib following a 1 mg/kg intravenous dose in rats is presented in Figure 6, with the corresponding pharmacokinetic parameters summarized in Table 5. After oral administration of lorlatinib, the plasma concentration increased sharply and the C_{max} of 468.02 ng/mL was reached at 1.36 h. The half-life

Table 4 The Main Pharmacokinetic Parameters of Lorlatinib After Oral Administration of Low, Medium and High Dose (5 mg/kg, 10 mg/kg and 50 mg/Kg) in Rats (n = 6)

Parameters	po. 5mg/kg	po. 10mg/kg	po. 50mg/kg
$t_{1/2z}$ (h)	5.00±2.07	8.82±3.97	17.58±20.27
T_{max} (h)	1.50±0.71	1.36±2.28	11.43±1.51
$CL_{z/F}$ (L/h)	0.003±0.001	0.004±0.003	0.001±0.001
$V_{z/F}$ (L/kg)	0.020±0.007	0.037±0.011	0.019±0.020
C_{max} (ng/mL)	218.29±72.67	468.02±165.79	2484.98±1363.21
$AUC_{(0–24h)}$ (ng h/mL)	1780.60±573.68	3162.09±1491.41	24,756.38±5906.92
$AUC_{(0-\infty)}$ (ng h/mL)	1871.87±679.45	3837.13±2157.00	92,790.77±54,229.49
$MRT_{(0–24h)}$ (h)	6.60±0.50	7.16±1.85	11.90±1.69
$MRT_{(0-\infty)}$ (h)	8.14±1.20	11.72±5.56	25.04±26.63

Notes: Values are expressed as mean ± SD.

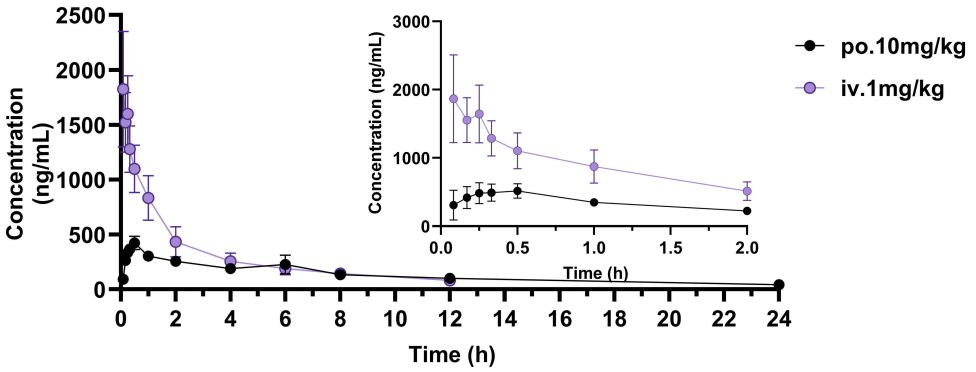

Figure 6 The mean plasma concentration time profile of lorlatinib after intravenous administration (1 mg/kg) (n = 6). The detailed plasma concentration-time profiles of lorlatinib during the initial 2 h period following administration was also showed. Error bars represent ± SD for concentrations.

($t_{1/2}$) was 8.82 h. Following intravenous administration, lorlatinib rapidly distributed to tissues and organs, resulting in a short $t_{1/2}$. The maximum plasma concentration of lorlatinib was 2,245.55 ng/mL, with a $t_{1/2}$ of 4.05 h. The $AUC_{(0–24h)}$ for the plasma concentration-time curve of lorlatinib was 3,162.09 ± 1,491.41 and 3,789.05 ± 2,316.59 ng h/mL for oral and intravenous administration, respectively. The absolute oral bioavailability of lorlatinib in rats was determined to be 8.58%, suggesting that lorlatinib may suffer from incomplete absorption in the gastrointestinal tract and/or could be extensively metabolized during first-pass metabolism.

Tissue Distribution

The tissue distribution of lorlatinib in rats after oral administration of 10 mg/kg is shown in Figure 7, with mean concentrations at different time points and corresponding tissue partition coefficients summarized in Table 6. Lorlatinib was detectable in all examined tissues as early as 0.083 h, indicating rapid systemic distribution. At 0.25 h, the highest concentration was observed in the stomach (22,850.67 ng/g), followed by the liver (3,893.61 ng/g), colon (2,772.92 ng/g), kidney (2,408.37 ng/g), heart (1,922.79 ng/g), lung (1,842.36 ng/g), cecum (1,498.22 ng/g), and spleen (1,323.12 ng/g). These results highlight the stomach as a major site of drug retention and the liver as the key organ for metabolism in rats.

Notably, lorlatinib has an exceptional capacity to penetrate the blood-brain barrier, as evidenced by a brain concentration of 774.29 ng/g and a brain-to-plasma ratio of 0.82. This underscores the potential contribution of its lipophilic nature to its in vivo disposition. The tissue partition coefficients detailed in Table 6 indicate that lorlatinib rapidly distributes to highly perfused organs in rats, including the liver (liver-to-plasma ratio = 4.82), kidneys (kidney-to-plasma ratio = 2.54), brain, and lungs (lung-to-plasma ratio = 1.77). This is consistent with its physicochemical properties and the expected distribution for lorlatinib.

Table 5 The Main Pharmacokinetic Parameters of Lorlatinib After Intravenous (1 mg/Kg) and Oral (10 mg/Kg) Administration in Rats (n = 6)

Parameters	po.10mg/kg	iv. 1mg/kg
$t_{1/2z}$ (h)	8.82±3.97	4.05±2.37
T_{max} (h)	1.36±2.28	0.13±0.07
CL (L/h)	0.004±0.003	–
Vz (L/kg)	0.037±0.011	0.002±0.001
C_{max} (ng/mL)	468.02±165.79	2245.55±1123.92
$AUC_{(0–24h)}$ (ng h/mL)	3162.09±1491.41	3789.05±2316.59
$AUC_{(0-\infty)}$ (ng h/mL)	3837.13±2157.00	4469.72±2543.95
$MRT_{(0–24h)}$ (h)	7.16±1.85	3.08±0.59
$MRT_{(0-\infty)}$ (h)	11.72±5.56	4.96±2.16

Notes: Values are expressed as mean ± SD.

https://doi.org/10.2147/DDDT.S565228

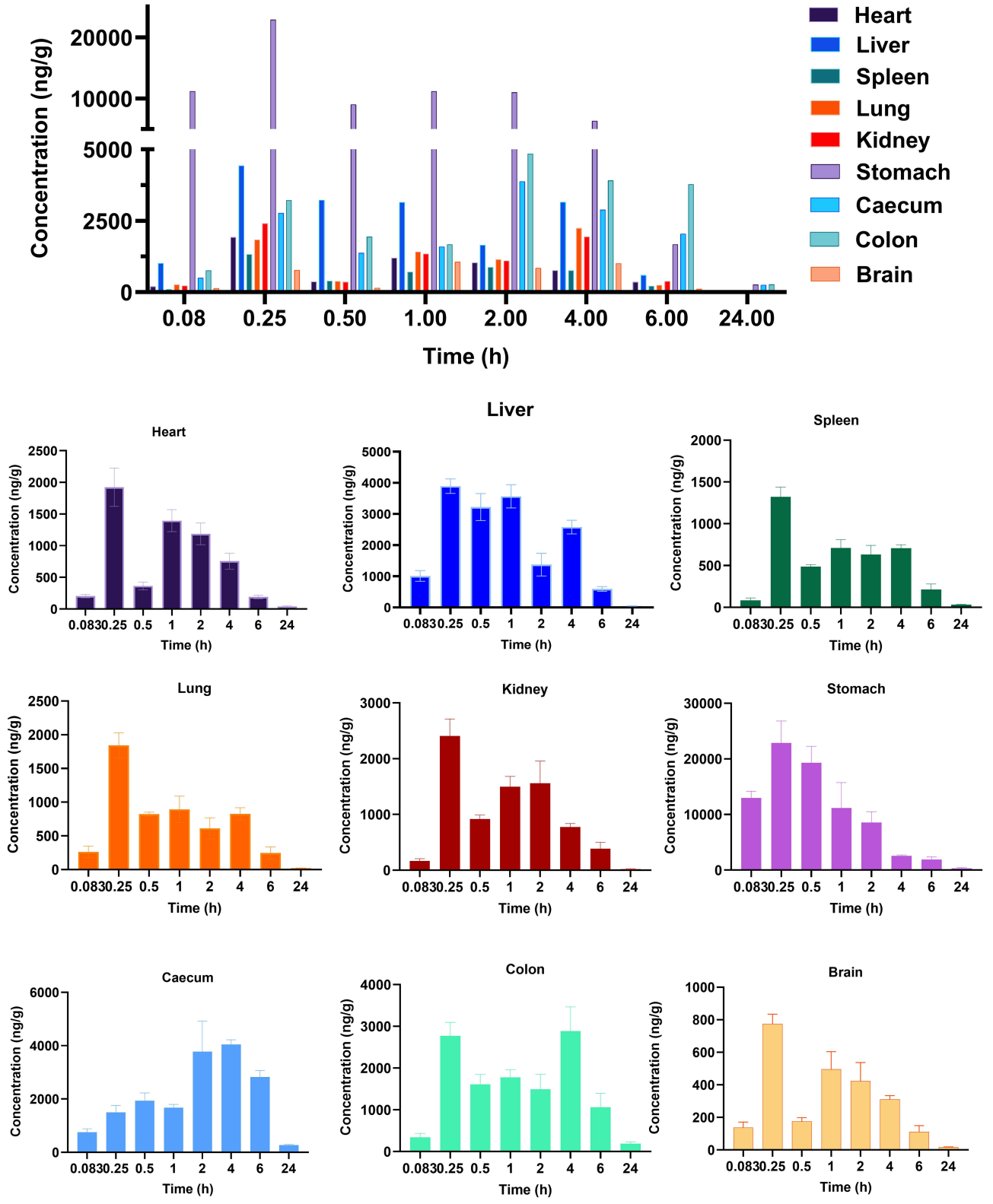

Figure 7 The mean drug concentrations in various tissues at different time points after oral administration at a dose of 10 mg/kg lorlatinib in rats (n = 6). Error bars represent ± SD for concentrations.

Table 6 Mean Tissue Concentrations at Various Time Points and Tissue Partition Coefficients Following a Single 10 mg/kg Oral Dose of Lorlatinib (n = 6)

Concentration (ng/g)	0.083h	0.25h	0.5h	1h	2h	4h	6h	24h	Kp
Heart	202.59	1922.79	363.25	1395.68	1186.16	756.31	189.59	40.59	0.54
Liver	1011.76	3893.61	3222.28	3565.25	1375.29	2579.56	594.86	47.90	4.82
Spleen	84.43	1323.12	486.99	710.04	630.27	708.31	213.03	31.80	1.59
Lung	262.42	1842.36	822.55	892.57	611.47	825.18	245.36	20.48	1.77
Kidney	163.32	2408.37	916.14	1497.35	1562.23	774.62	383.22	18.70	2.54
Stomach	12967.88	22,850.67	19,278.43	11,188.84	8560.65	2574.29	1916.67	316.48	15.47
Caecum	759.56	1498.22	1937.34	1675.63	3776.55	4049.29	2820.78	272.79	12.89
Colon	341.54	2772.92	1611.76	1775.75	1490.22	2884.30	1062.41	188.67	7.15
Brain	137.73	774.29	175.23	495.49	423.77	310.81	110.84	16.45	0.82

Notes: Kp =$AUC_{(0-\infty)}$, tissue/$AUC_{(0-\infty)}$, plasma. Values are expressed as mean.

Molecular Docking

To corroborate the inhibitory effects of itraconazole and voriconazole on lorlatinib metabolism, we performed molecular docking studies. As depicted in Figure 8, lorlatinib as well as both azoles were predicted to occupy the catalytic pocket of CYP3A4. Itraconazole established hydrogen bonds with ARG-372 (3.5 Å and 2.3 Å), ARG-212 (2.8 Å) and ILE-300 (3.2 Å), whereas voriconazole interacted with ASP-76 (2.8 Å), ARG-106 (2.3 Å), THR-224 (2.5 Å), and LEU-221 (3.4 Å). Lorlatinib also showed interactions with THR-224 (3.3 Å), GLY-109 (2.6 Å), and PHE-108 (3.2 Å). The calculated binding energies were −10.63 kcal/mol for voriconazole, −8.82 kcal/mol for lorlatinib, and −7.80 kcal/mol for itraconazole. Collectively, these docking data demonstrate strong CYP3A4 binding by itraconazole and voriconazole, offering a plausible mechanistic basis for their observed inhibition of lorlatinib metabolism in vivo. Furthermore, detailed two-dimensional ligand–protein interaction diagrams of CYP3A4 with lorlatinib, itraconazole, and voriconazole are provided in the Supplementary Figures 5–7. These 2D diagrams comprehensively illustrate all types of ligand–enzyme interactions, including hydrogen bonds, hydrophobic contacts, and π-related interactions, highlighting the specific residues involved in binding.

Discussion

This study provides a comprehensive characterization of lorlatinib's pharmacokinetics, integrating in vitro metabolism with in vivo disposition. Notably, this is the first study to employ M2a as a representative marker metabolite to characterize lorlatinib metabolism in liver microsomes. M2a was selected because it exhibited a stable and reproducible response in our assays, whereas among the three known in vitro metabolites reported in the FDA documentation,[34] M6 is formed exclusively via CYP3A4 and M1a through UGT-mediated conjugation, both showing responses below the quantification limit, making M2a the most suitable indicator of overall microsomal metabolic activity (Supplementary Figures 1 and 2).

In this study, it was first observed that lorlatinib undergoes rapid metabolism in RLM, as evidenced by the low K_m value of 0.035 mM and the high C_{Lint} of 68.27 pmol/mg/min, suggesting efficient metabolic processing in rats and a high enzyme-substrate binding affinity. In contrast, HLM exhibited a significantly higher K_m of 2.552 mM and a lower C_{Lint} of 3.41 μL/min/mg protein, indicating a reduced affinity for the substrate and slower metabolic clearance in humans. These metabolic differences not only suggest that lorlatinib metabolism is much slower in humans than in rats, but also imply the potential for drug accumulation in plasma and tissues, particularly when the drug is highly lipophilic (Supplementary Table 5). Such accumulation could increase the risk of toxicity due to increased systemic exposure and may lead to higher accumulation in highly perfused organs.[35] Additionally, the significant differences observed in K_m and CL_{int} between rats and humans also highlight the importance of understanding species-specific metabolic processes. These differences underscore the necessity of carefully interpreting preclinical pharmacokinetics to avoid overestimating clearance in animal models, which may not accurately predict human drug behavior.[36]

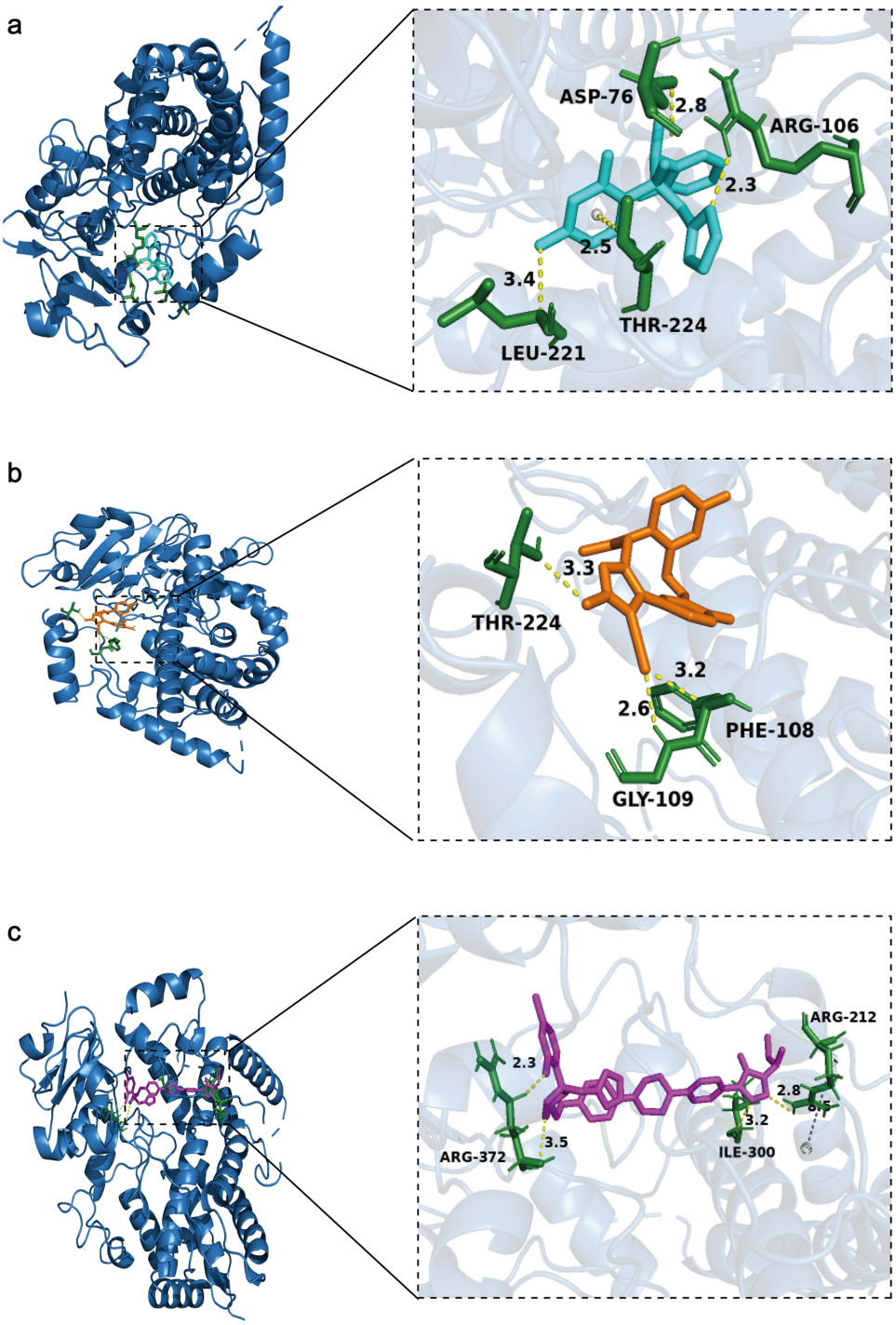

Figure 8 Molecular docking of lorlatinib and azoles with CYP3A4. (**a**) Voriconazole, (**b**) lorlatinib, and (**c**) itraconazole were docked into the CYP3A4 catalytic pocket. Key hydrogen bond interactions are indicated. The binding energies were −10.63, −8.82, and −7.80 kcal/mol, respectively, supporting strong CYP3A4 affinity of the azoles consistent with their inhibitory effects in vivo.

Therefore, to further explore the metabolic differences caused by species-specific metabolism of lorlatinib in vivo, the contribution of various cytochrome P450 (CYP) enzymes was assessed using probe substrate assays in both HLM and RLM. While CYP3A4 remains the primary enzyme in both rats and humans, notable divergence was observed for CYP2C19. In rat liver microsomes, CYP2C19 contributed substantially to lorlatinib metabolism, whereas in human liver microsomes its activity was almost negligible. These interspecies differences not only affect overall metabolic clearance

but may also influence the relative impact of CYP-specific inhibitors or inducers, emphasizing the importance of integrating species-specific enzyme phenotyping into pharmacokinetic assessments.

The trends observed in our study were consistent with clinical findings reported by Zhou et al and Umehara et al, where rifampicin markedly reduced lorlatinib exposure due to CYP3A induction, while itraconazole increased systemic exposure through potent CYP3A inhibition.[13,14] Interestingly, unlike in humans, the inhibitory effects of CYP3A inhibitors on lorlatinib metabolism differed markedly in rats, with voriconazole exerting a stronger impact than itraconazole. Although itraconazole is generally recognized as a potent time-dependent CYP3A4 inhibitor in clinical settings,[37] our findings are consistent with a previous pharmacokinetic study reporting a greater effect of voriconazole in vivo.[38] This apparent discrepancy can be explained by differences in their inhibitory spectrum and pharmacokinetic characteristics. Voriconazole, a broad-spectrum triazole, is known to strongly inhibit CYP2C19 and CYP2C9 and moderately inhibit CYP3A4.[37] Its high oral bioavailability and relatively low plasma protein binding facilitate higher free drug exposure in rats, thereby enhancing CYP3A4 inhibition.[39–41] By contrast, itraconazole, despite being a strong CYP3A4 inhibitor, has poor solubility, pH-dependent absorption, and extremely high protein binding (~99%), which limit the free drug concentration available to act on CYP3A4.[42] Consistently, in silico predictions from SwissADME aligned with these physicochemical differences, further supporting their divergent inhibitory effects observed in vivo (Supplementary Table 5). These factors, together with potential differences in transporter interactions and species-specific pharmacokinetics, likely account for the more modest inhibitory effect of itraconazole observed in our study.

Notably, human clinical pharmacology data show that lorlatinib is not only a substrate of CYP3A4 but also exhibits time-dependent inhibition and induction of CYP3A, which may further complicate its interaction profile in vivo.[43] Importantly, in a Phase I human study, co-administration of itraconazole (200 mg/day) with a single dose of lorlatinib (100 mg) increased lorlatinib $AUC_{(0-\infty)}$ by ~141.8% and C_{max} by ~124.4% compared with lorlatinib alone, confirming itraconazole as a strong clinical inhibitor of CYP3A4.[13] Collectively, these findings emphasize the need for caution when extrapolating rat data to humans and suggest that voriconazole may pose a greater inhibitory risk in preclinical models, whereas itraconazole remains the more potent inhibitor in clinical practice.

Molecular docking analysis provided mechanistic support for these observations. Voriconazole exhibited stronger binding affinity for the CYP3A4 active site compared with lorlatinib, indicating its ability to effectively compete for the binding pocket and suppress metabolism. In contrast, itraconazole showed slightly weaker affinity but formed multiple hydrogen bonds, consistent with its moderate inhibitory effect in microsomal assays. Together, these results suggest that co-administration with CYP3A inhibitors can substantially increase lorlatinib exposure, although the extent of interaction may vary depending on the inhibitor and the experimental system. Since most inducers exert their effects by activating nuclear receptors like pregnane X receptor (PXR) and constitutive androstane receptor (CAR), which upregulate CYP3A4 expression at the transcriptional level rather than directly binding to the CYP3A4 active site, molecular docking simulations of lorlatinib with inducers were not conducted in this study.[44]

Therefore, we focused on studying the effects of co-administration with inducers in rats, specifically assessing how these compounds influence lorlatinib's pharmacokinetics. In comparison to lorlatinib administered alone, co-administration with rifampicin significantly reduced the C_{max}, $AUC_{(0–24h)}$, and $AUC_{(0-\infty)}$ by 70.07%, 77.12%, and 80.31%, respectively. These findings are consistent with their underlying mechanisms. Rifampicin, a potent PXR activator, strongly induces CYP3A4 and intestinal P-gp, while carbamazepine activates both PXR and CAR, leading to broader but less selective induction.[45] Taken together, these results highlight co-administration of lorlatinib with strong CYP3A4 inducers such as rifampicin or carbamazepine is strictly contraindicated.

Building on the significant role of CYP3A4 in lorlatinib metabolism observed in our pharmacokinetics studies, we next examined its dose-dependent pharmacokinetic behavior in rats. To this end, lorlatinib was administered at 5, 10, and 50 mg/kg to evaluate systemic exposure. These results indicate a trend toward nonlinear pharmacokinetics at 50 mg/kg, which may be related to partial saturation of CYP3A4-mediated metabolism; however, confirmation of nonlinear kinetics would require further evaluation across a broader dose range. Because of species differences in clearance, protein binding, and bioavailability, direct milligram-per-kilogram conversion between humans and rats is inappropriate.[46,47]

To further investigate this possibility under conventional exposure conditions, we next evaluated the tissue distribution of lorlatinib in rats at 10 mg/kg. The analysis was performed at key time points (0.083, 0.25, 0.5, 1, 2, 4, 6, and

24 hours post-administration) designed to characterize lorlatinib concentrations in various tissues across the pre-peak, peak, and post-peak phases of plasma concentration. Lorlatinib levels in the stomach peaked at 22,850.67 ng/g at 0.25 h, reflecting efficient dissolution and initial absorption, while the subsequent decline in liver concentrations (3,893.61 → 47.90 ng/g) suggested its central role in clearance, likely through metabolism and high hepatic blood flow.[48] Similarly, lorlatinib concentrations in the cecum and colon decreased markedly, consistent with the intestine contributing to drug elimination via both metabolic and efflux mechanisms.[49] These findings, together with the calculated oral bioavailability of 8.58%, indicate that extensive first-pass processes in the liver and intestine substantially limit systemic exposure. Notably, most tissues exhibited a secondary peak at 2–4 h, which may reflect redistribution from lipophilic tissues, whereas the delayed peak in the cecum and colon is more plausibly explained by gastrointestinal transit and reabsorption.[50,51] Such redistribution and delayed gastrointestinal transit and reabsorption could contribute to gastrointestinal adverse effects commonly observed in NSCLC patients receiving lorlatinib.[52]

An assessment of lorlatinib's distribution and behavior across tissues was carried out using the partition coefficient (Kp) to evaluate tissue-to-plasma ratios.[53] Among all tissues, the brain distribution is of particular clinical relevance, given the high incidence of brain metastases in NSCLC patients. Lorlatinib achieved a peak brain concentration of 774.29 ng/g at 0.25 hours, corresponding to a brain-to-plasma ratio of 0.82, which demonstrates efficient penetration across the blood–brain barrier.[54] This property distinguishes lorlatinib from earlier-generation ALK inhibitors such as crizotinib, which exhibits a much lower brain-to-plasma ratio of 0.23.[55] Notably, interspecies differences were also observed, with wild-type mice showing a brain-to-plasma ratio of approximately 0.5–0.6, whereas in humans a cerebrospinal fluid-to-plasma concentration ratio of 0.77 has been reported.[56,57] Although the clinical value is derived from cerebrospinal fluid rather than brain tissue directly, these data are broadly consistent with our findings and support lorlatinib's strong central nervous system penetration across species.

Additionally, transporter interactions may significantly influence lorlatinib disposition. Lorlatinib has been reported as a substrate of P-gp/ABCB1 (and to a lesser extent ABCG2) at the blood–brain barrier,[56] while in vitro studies suggest potential inhibition of uptake transporters such as OCT1, OAT3, and OATPs;[34] however, definitive evidence for the role of hepatic uptake transporters in vivo remains limited. Collectively, these observations indicate that in vivo drug–drug interactions cannot be attributed solely to CYP3A4 modulation, and transporter-mediated processes likely act in concert with metabolism, warranting further mechanistic evaluation. Although the present study focused primarily on Phase I oxidative metabolism, future investigations should also examine Phase II pathways, such as UGT1A4-mediated conjugation, to achieve a more complete understanding of lorlatinib clearance. Moreover, because NSCLC patients receive lorlatinib once daily, single-dose pharmacokinetic studies have inherent limitations, and the impact of chronic dosing—particularly given lorlatinib's dual role as a both a time-dependent inhibitor and an inducer of CYP3A—merits further study to assess potential time-dependent changes in systemic exposure.[3,43]

In conclusion, this study provides novel insights into the metabolism, pharmacokinetics, and tissue distribution of lorlatinib, emphasizing the central role of CYP3A4 in its disposition and drug–drug interaction potential. A more comprehensive understanding of lorlatinib's pharmacokinetic profile will support the optimization of treatment strategies and guide personalized therapy to maximize both safety and efficacy.

Conclusion

This study comprehensively evaluated the metabolism, pharmacokinetics, and tissue distribution of lorlatinib in rats using both in vitro and in vivo approaches. Lorlatinib was found to undergo extensive CYP3A4-mediated metabolism, exhibiting low oral bioavailability and nonlinear pharmacokinetics. Coadministration with CYP3A4 inhibitors markedly increased systemic exposure, whereas inducers significantly reduced it, highlighting a high potential for drug–drug interactions. Lorlatinib was widely distributed across major organs and showed efficient brain penetration, consistent with its clinical efficacy against CNS metastases. These findings provide mechanistic insights into lorlatinib disposition and underscore the need for careful management of CYP3A4-mediated interactions in clinical practice.

Abbreviations

ALK, Anaplastic Lymphoma Kinase; ANOVA, Analysis of Variance; ARG, Arginine; AUC, Area Under the Curve; BBB, Blood–Brain Barrier; CAR, Constitutive Androstane Receptor; CNS, Central Nervous System; CSF, Cerebrospinal Fluid; CYP, Cytochrome P450; DDI, Drug–Drug Interaction; DMSO, Dimethyl Sulfoxide; FMO, Flavin-Containing Monooxygenase; HLM, Human Liver Microsomes; i.v., Intravenous; UHPLC–MS/MS, Ultra-High-Performance Liquid Chromatography–Tandem Mass Spectrometry; LFT, Liver Function Test; MRT, Mean Residence Time; NADPH, Nicotinamide Adenine Dinucleotide Phosphate; NSCLC, Non-Small Cell Lung Cancer; P-gp, P-Glycoprotein; PK, Pharmacokinetics; PXR, Pregnane X Receptor; QC, Quality Control; ROS1, c-ros Oncogene 1; SD, Standard Deviation; TKI, Tyrosine Kinase Inhibitor; $t_{1/2}$, Elimination Half-Life; T_{max}, Time to Reach Maximum Concentration; UGT, UDP-Glucuronosyltransferase; V_{max}, Maximum Velocity (of an Enzymatic Reaction); $V_{z/F}$, Volume of Distribution.

Data Sharing Statement

The data supporting the findings of this study are available from the corresponding author upon reasonable request.

Ethics Statement

All animal experiments were conducted in compliance with the Guide for the Care and Use of Laboratory Animals and approved by the Institutional Animal Care and Use Committee of Southern Medical University (Approval No. SMUL202410030).

Acknowledgments

The authors thank the staff of the Experimental Animal Center of Southern Medical University for their support with animal care and handling. We also acknowledge the technical assistance provided by the Clinical Pharmacy Center for UHPLC-MS/MS measurements.

Author Contributions

Cong Xie and Tongshu Guan contributed equally to this work and share first authorship. Yilei Li and Ping Zheng are co-corresponding authors. Conceptualization: Cong Xie and Tongshu Guan, Yilei Li and Ping Zheng; Methodology: Cong Xie and Tongshu Guan; Investigation: Jin Huang, Jiayu Chen; Formal analysis: Jin Huang, Jiayu Chen; Data curation: Jin Huang, Jiayu Chen; Writing – original draft: Cong Xie and Tongshu Guan; Writing – review & editing: Yilei Li and Ping Zheng; Supervision: Yilei Li and Ping Zheng; Funding acquisition: Cong Xie. All authors made a significant contribution to the work reported, whether that is in the conception, study design, execution, acquisition of data, analysis and interpretation, or in all these areas; took part in drafting, revising or critically reviewing the article; gave final approval of the version to be published; have agreed on the journal to which the article has been submitted; and agree to be accountable for all aspects of the work.

Funding

This work was supported by the National Natural Science Foundation of China [82204499], the China International Medical Foundation [Z-2021-46-2101], Science and Technology Program of Guangzhou [2025A04J4279] and the Science and Technology Projects in Guangzhou [202201010876].

Disclosure

The authors report no conflicts of interest in this work.

References

1. Syed YY. Lorlatinib: first Global Approval. *Drugs*. 2019;79(1):93–98. doi:10.1007/s40265-018-1041-0
2. Pfizer. LORBRENA® (lorlatinib): prescribing information. https://labeling.pfizer.com/ShowLabeling.aspx?id=11140. Accessed Aug 13, 2025.
3. Chen J, O'Gorman MT, James LP, Klamerus KJ, Mugundu G, Pithavala YK. Pharmacokinetics of Lorlatinib After Single and Multiple Dosing in Patients with Anaplastic Lymphoma Kinase (ALK)-Positive Non-Small Cell Lung Cancer: results from a Global Phase I/II Study. *Clin Pharmacokinet*. 2021;60(10):1313–1324. doi:10.1007/s40262-021-01015-z

4. Hussaarts KGAM, Veerman GDM, Jansman FGA, van Gelder T, Mathijssen RHJ, van Leeuwen RWF. Clinically relevant drug interactions with multikinase inhibitors: a review. *Therapeut Adv Med Oncol*. 2019;11:1758835918818347. doi:10.1177/1758835918818347
5. Calles A, Alonso M, Martín-Martorell P, et al. Efficacy and safety of lorlatinib in patients with ALK- and ROS1-rearranged metastatic non-small cell lung cancer treated within the compassionate use program in Spain. *Cancer Treat Res Commun*. 2025;43:100905. doi:10.1016/j.ctarc.2025.100905
6. Chen J, Ruiz-Garcia A, James LP, et al. Lorlatinib Exposure-Response Analyses for Safety and Efficacy in a Phase I/II Trial to Support Benefit-Risk Assessment in Non-Small Cell Lung Cancer. *Clin Pharmacol Ther*. 2021;110(5):1273–1281. doi:10.1002/cpt.2228
7. Eichelbaum M, Burk O. CYP3A genetics in drug metabolism. *Nature Med*. 2001;7(3):285–287. doi:10.1038/85417
8. Mikus G, Isabelle Foerster K. Role of CYP3A4 in kinase inhibitor metabolism and assessment of CYP3A4 activity. *Transl Cancer Res*. 2017;6(S10):S1592–S1599. doi:10.21037/tcr.2017.09.10
9. Molenaar-Kuijsten L, Van Balen DEM, Beijnen JH, Steeghs N, Huitema ADR. A Review of CYP3A Drug-Drug Interaction Studies: practical Guidelines for Patients Using Targeted Oral Anticancer Drugs. *Front Pharmacol*. 2021;12:670862. doi:10.3389/fphar.2021.670862
10. Dutreix C, Peng B, Mehring G, et al. Pharmacokinetic interaction between ketoconazole and imatinib mesylate (Glivec) in healthy subjects. *Cancer Chemother Pharmacol*. 2004;54(4):290–294. doi:10.1007/s00280-004-0832-z
11. Tugnait M, Gupta N, Hanley MJ, et al. Effects of Strong CYP2C8 or CYP3A Inhibition and CYP3A Induction on the Pharmacokinetics of Brigatinib, an Oral Anaplastic Lymphoma Kinase Inhibitor, in Healthy Volunteers. *Clin Pharmacol Drug Dev*. 2020;9(2):214–223. doi:10.1002/cpdd.723
12. Vishwanathan K, Dickinson PA, So K, et al. The effect of itraconazole and rifampicin on the pharmacokinetics of osimertinib. *Br J Clin Pharmacol*. 2018;84(6):1156–1169. doi:10.1111/bcp.13534
13. Patel M, Chen J, McGrory S, et al. The effect of itraconazole on the pharmacokinetics of lorlatinib: results of a Phase I, open-label, crossover study in healthy participants. *Invest New Drugs*. 2020;38(1):131–139. doi:10.1007/s10637-019-00872-7
14. Chen J, Xu H, Pawlak S, et al. The Effect of Rifampin on the Pharmacokinetics and Safety of Lorlatinib: results of a Phase One, Open-Label, Crossover Study in Healthy Participants. *Adv Ther*. 2020;37(2):745–758. doi:10.1007/s12325-019-01198-9
15. Ibrahim SM, Pithavala YK, Vourvahis M, Chen J. A literature review of liver function test elevations in rifampin drug-drug interaction studies. *Clin Transl Sci*. 2022;15(7):1561–1580. doi:10.1111/cts.13281
16. Hu W, Lettiere D, Tse S, et al. Liver Toxicity Observed With Lorlatinib When Combined With Strong CYP3A Inducers: evaluation of Cynomolgus Monkey as a Nonclinical Model for Assessing the Mechanism of Combinational Toxicity. *Toxicol Sci*. 2021;182(2):183–194. doi:10.1093/toxsci/kfab056
17. Stypinski D, Fostvedt L, Lam JL, et al. Metabolism, Excretion, and Pharmacokinetics of Lorlatinib (PF-06463922) and Evaluation of the Impact of Radiolabel Position and Other Factors on Comparability of Data Across 2 ADME Studies. *J Clin Pharmacol*. 2020;60(9):1254–1267. doi:10.1002/jcph.1621
18. Chen J, Bearz A, Kim DW, et al. Evaluation of the Effect of Lorlatinib on CYP2B6, CYP2C9, UGT, and P-Glycoprotein Substrates in Patients with Advanced Non-Small Cell Lung Cancer. *Clin Pharmacokinet*. 2024;63(2):171–182. doi:10.1007/s40262-023-01309-4
19. Zhao D, Chen J, Chu M, Long X, Wang J. Pharmacokinetic-Based Drug-Drug Interactions with Anaplastic Lymphoma Kinase Inhibitors: a Review. *Drug Des Devel Ther*. 2020;14:1663–1681. doi:10.2147/dddt.S249098
20. Wang X, He B, Shi J, Li Q, Zhu HJ. Comparative Proteomics Analysis of Human Liver Microsomes and S9 Fractions. *Drug Metab Dispos*. 2020;48(1):31–40. doi:10.1124/dmd.119.089235
21. Asha S, Vidyavathi M. Role of Human Liver Microsomes in In Vitro Metabolism of Drugs—A Review. *Appl Biochem Biotechnol*. 2010;160(6):1699–1722. doi:10.1007/s12010-009-8689-6
22. Knights KM, Stresser DM, Miners JO, Crespi CL. In Vitro Drug Metabolism Using Liver Microsomes. *Curr Protoc Pharmacol*. 2016;74(1):7.8.1–7.8.24. doi:10.1002/cpph.9
23. Obach RS. Prediction of human clearance of twenty-nine drugs from hepatic microsomal intrinsic clearance data: an examination of in vitro half-life approach and nonspecific binding to microsomes. *Drug Metab Dispos*. 1999;27(11):1350–1359. doi:10.1016/S0090-9556(24)14938-0
24. Marothu VK, Padmalatha K, Madhavi G. In vitro Metabolic Stability of Drugs and Applications of LC-MS in Metabolite Profiling. In: Dunnington K, editor. *Drug Metabolism*. IntechOpen; 2021.
25. Yuan W, Shi G, Gou L, Yang J. Metabolic Profiling of Canertinib: a Comprehensive Cross-Species Investigation Using Advanced UPLC-MS/MS and LC-Orbitrap-HRMS Techniques. *Biomed Chromatogr*. 2025;39(8):e70157. doi:10.1002/bmc.70157
26. Jiang S, Li X, Xue W, et al. Preclinical pharmacokinetic characterization of amdizalisib, a novel PI3Kδ inhibitor for the treatment of hematological malignancies. *Front Pharmacol*. 2024;15:1392209. doi:10.3389/fphar.2024.1392209
27. Zapata Dongo RJ, Poterico JA, Fontana D, et al. An in silico evaluation of lorlatinib as a potential therapy for novel amino acid substitutions in the tyrosine kinase domain of the ALK protein associated with cancer. *Brief Research Report Front Pharmacol*. 2025;16:314. doi:10.3389/fphar.2025.1605314
28. Tang C, Niu X, Shi L, Zhu H, Lin G, Xu RA. In vivo Pharmacokinetic Drug-Drug Interaction Studies Between Fedratinib and Antifungal Agents Based on a Newly Developed and Validated UPLC/MS-MS Method. *Front Pharmacol*. 2020;11:626897. doi:10.3389/fphar.2020.626897
29. Yang S, Zhang X, Wang Y, et al. Development of UPLC-MS/MS Method for Studying the Pharmacokinetic Interaction Between Dasatinib and Posaconazole in Rats. *Drug Des Devel Ther*. 2021;15:2171–2178. doi:10.2147/dddt.S301241
30. Lou D, Cui X, Bao SS, et al. Effects of ketoconazole, voriconazole, and itraconazole on the pharmacokinetics of apatinib in rats. *Drug Dev Ind Pharm*. 2019;45(4):689–693. doi:10.1080/03639045.2019.1569042
31. Yamashita F, Sasa Y, Yoshida S, et al. Modeling of Rifampicin-Induced CYP3A4 Activation Dynamics for the Prediction of Clinical Drug-Drug Interactions from In Vitro Data. *PLoS One*. 2013;8(9):e70330. doi:10.1371/journal.pone.0070330
32. Tateishi T, Asoh M, Nakura H, et al. Carbamazepine induces multiple cytochrome P450 subfamilies in rats. *Chem Biol Interact*. 1999;117(3):257–268. doi:10.1016/s0009-2797(98)00110-0
33. Lin Y, Lu P, Tang C, et al. Substrate inhibition kinetics for cytochrome P450-catalyzed reactions. *Drug Metab Dispos*. 2001;29(4):368–374.
34. FDA. *LORBRENA® (lorlatinib) tablets prescribing information*. 2021. https://www.accessdata.fda.gov/drugsatfda_docs/label/2021/210868s004lbl.pdf. Accessed Sep 20, 2025.

35. Chen W, Shi Y, Qi S, et al. Pharmacokinetic Study and Tissue Distribution of Lorlatinib in Mouse Serum and Tissue Samples by Liquid Chromatography-Mass Spectrometry. *J Anal Methods Chem*. 2019;2019:7574369. doi:10.1155/2019/7574369
36. Abass K, Reponen P, Anyanwu B, Pelkonen O. Inter-species differences between humans and other mammals in the in vitro metabolism of carbofuran and the role of human CYP enzymes. *Environ Toxicol Pharmacol*. 2023;102:104243. doi:10.1016/j.etap.2023.104243
37. Brüggemann RJM, Alffenaar J-WC, Blijlevens NMA, et al. Clinical Relevance of the Pharmacokinetic Interactions of Azole Antifungal Drugs with Other Coadministered Agents. *Clin Infect Dis*. 2009;48(10):1441–1458. doi:10.1086/598327
38. Ye Z, Wang C, Li R, et al. Potential interactions between triazole antifungal agents and lorlatinib based on ultra-performance liquid chromatography-tandem mass spectrometry in rat plasma. *J Pharm Pharmacol*. 2024;76(2):115–121. doi:10.1093/jpp/rgad105
39. Yu H-M, Zhang B-X, Xing W-H, et al. Investigation into the structures and physicochemical properties of multi-component crystals of voriconazole. *Chin Chem Lett*. 2023;34(6):107668. doi:10.1016/j.cclet.2022.07.011
40. Rauseo AM, Mazi P, Lewis P, Burnett B, Mudge S, Spec A. Bioavailability of Single-Dose SUBA-Itraconazole Compared to Conventional Itraconazole under Fasted and Fed Conditions. *Antimicrob Agents Chemother*. 2021;65(8):e0013421. doi:10.1128/aac.00134-21
41. Schueller O, Willson A, Singh N, Lohmer L, Alabanza A, Patel J. A Phase 1 Pharmacokinetic Drug Interaction Study of Belumosudil Coadministered With CYP3A4 Inhibitors and Inducers and Proton Pump Inhibitors. *Clin Pharmacol Drug Dev*. 2022;11(7):795–806. doi:10.1002/cpdd.1082
42. Bellmann R, Smuszkiewicz P. Pharmacokinetics of antifungal drugs: practical implications for optimized treatment of patients. *Infection*. 2017;45(6):737–779. doi:10.1007/s15010-017-1042-z
43. Hibma JE, O'Gorman M, Nepal S, Pawlak S, Ginman K, Pithavala YK. Evaluation of the absolute oral bioavailability of the anaplastic lymphoma kinase/c-ROS oncogene 1 kinase inhibitor lorlatinib in healthy participants. *Cancer Chemother Pharmacol*. 2022;89(1):71–81. doi:10.1007/s00280-021-04368-1
44. Kobayashi K, Kuze J, Abe S, et al. CYP3A4 Induction in the Liver and Intestine of Pregnane X Receptor/CYP3A-Humanized Mice: approaches by Mass Spectrometry Imaging and Portal Blood Analysis. *Mol Pharmacol*. 2019;96(5):600–608. doi:10.1124/mol.119.117333
45. Pan X, Yamazaki S, Neuhoff S, Zhang M, Pilla Reddy V. Unraveling pleiotropic effects of rifampicin by using physiologically based pharmacokinetic modeling: assessing the induction magnitude of P-glycoprotein-cytochrome P450 3A4 dual substrates. *CPT Pharmacometrics Syst Pharmacol*. 2021;10(12):1485–1496. doi:10.1002/psp4.12717
46. Reagan-Shaw S, Nihal M, Ahmad N. Dose translation from animal to human studies revisited. *FASEB j*. 2008;22(3):659–661. doi:10.1096/fj.07-9574LSF
47. Chen Y, Zhou Z, Zeng Y, et al. Interaction study between HIV protease inhibitors and alectinib in rats based on an ultra-performance liquid chromatography tandem mass spectrometry method. *J Chromatogr B Analyt Technol Biomed Life Sci*. 2025;1253:124483. doi:10.1016/j.jchromb.2025.124483
48. Zhao J, Yuan W, Wang S, et al. Comparative Pharmacokinetics and Tissue Distribution of M10 and Its Metabolite Myricetin in Normal and Dextran-Sodium-Sulfate-Induced Colitis Mice. *Molecules*. 2022;27(23):8140. doi:10.3390/molecules27238140
49. Lu J-Z, Hong -D-D, Ye D, et al. Tissue distribution and integrated pharmacokinetic properties of major effective constituents of oral Gegen-Qinlian decoction in mice. *Front Pharmacol*. 2022;13. doi:10.3389/fphar.2022.996143
50. Metsugi Y, Ogawara K-I, Higaki K, Kimura T, Kimura T. Appearance of Double Peaks in Plasma Concentration–time Profile after Oral Administration Depends on Gastric Emptying Profile and Weight Function. *Pharm Res*. 2008;25(4):886–895. doi:10.1007/s11095-007-9469-z
51. Davies N, Takemoto J, Brocks D, Yáñez J. Multiple Peaking Phenomena in Pharmacokinetic Disposition. *Clin Pharmacokinet*. 2010;49(6):351–377. doi:10.2165/11319320-000000000-00000
52. Bauer TM, Felip E, Solomon BJ, et al. Clinical Management of Adverse Events Associated with Lorlatinib. *Oncologist*. 2019;24(8):1103–1110. doi:10.1634/theoncologist.2018-0380
53. Rijmers J, Sparidans RW, Acda M, et al. Brain Exposure to the Macrocyclic ALK Inhibitor Zotizalkib is Restricted by ABCB1, and Its Plasma Disposition is Affected by Mouse Carboxylesterase 1c. *Mol Pharm*. 2024;21(10):5159–5170. doi:10.1021/acs.molpharmaceut.4c00542
54. Bauer TM, Shaw AT, Johnson ML, et al. Brain Penetration of Lorlatinib: cumulative Incidences of CNS and Non-CNS Progression with Lorlatinib in Patients with Previously Treated ALK-Positive Non-Small-Cell Lung Cancer. *Target Oncol*. 2020;15(1):55–65. doi:10.1007/s11523-020-00702-4
55. Tang SC, Nguyen LN, Sparidans RW, Wagenaar E, Beijnen JH, Schinkel AH. Increased oral availability and brain accumulation of the ALK inhibitor crizotinib by coadministration of the P-glycoprotein (ABCB1) and breast cancer resistance protein (ABCG2) inhibitor elacridar. *Int J Cancer*. 2014;134(6):1484–1494. doi:10.1002/ijc.28475
56. Li W, Sparidans RW, Wang Y, et al. P-glycoprotein (MDR1/ABCB1) restricts brain accumulation and cytochrome P450-3A (CYP3A) limits oral availability of the novel ALK/ROS1 inhibitor lorlatinib. *Int J Cancer*. 2018;143(8):2029–2038. doi:10.1002/ijc.31582
57. Sun S, Pithavala YK, Martini JF, Chen J. Evaluation of Lorlatinib Cerebrospinal Fluid Concentrations in Relation to Target Concentrations for Anaplastic Lymphoma Kinase (ALK) Inhibition. *J Clin Pharmacol*. 2022;62(9):1170–1176. doi:10.1002/jcph.2056

Drug Design, Development and Therapy

Dovepress
Taylor & Francis Group

Publish your work in this journal

Drug Design, Development and Therapy is an international, peer-reviewed open-access journal that spans the spectrum of drug design and development through to clinical applications. Clinical outcomes, patient safety, and programs for the development and effective, safe, and sustained use of medicines are a feature of the journal, which has also been accepted for indexing on PubMed Central. The manuscript management system is completely online and includes a very quick and fair peer-review system, which is all easy to use. Visit http://www.dovepress.com/testimonials.php to read real quotes from published authors.

Submit your manuscript here: https://www.dovepress.com/drug-design-development-and-therapy-journal